RESEARCH ARTICLE | DECEMBER 08 2023

Consistent energy-based framework of amplification mechanisms for the second mode in hypersonic boundary layers

Yifeng Chen (陈亦锋) ; Peixu Guo (郭培旭) ; Chihyung Wen (温志湧)

Physics of Fluids 35, 124107 (2023)
https://doi.org/10.1063/5.0176245

Physics of Fluids ARTICLE pubs.aip.org/aip/pof

Consistent energy-based framework of amplification mechanisms for the second mode in hypersonic boundary layers

Cite as: Phys. Fluids **35**, 124107 (2023); doi: 10.1063/5.0176245
Submitted: 12 September 2023 · Accepted: 20 November 2023 ·
Published Online: 8 December 2023

Yifeng Chen (陈亦锋),[a] Peixu Guo (郭培旭),[b] and Chihyung Wen (温志湧)

AFFILIATIONS

Department of Aeronautical and Aviation Engineering, The Hong Kong Polytechnic University, Kowloon, Hong Kong, China

[a]Electronic mail: yi-feng.chen@connect.polyu.hk
[b]Author to whom correspondence should be addressed: peixu.guo@outlook.com

ABSTRACT

The second mode is of general interest in hypersonic boundary layer flows due to its underlying responsibilities for transition to turbulence. However, a long-term debate exists on the detailed energy sources that sustain the modal exponential growth. Currently, three influential energy-based approaches appear to show different significant energy sources due to dissimilar mathematical formulations, including the momentum potential theory, the inviscid Lagrangian energy analysis, and the relative phase analysis. In this study, these three fundamental approaches are employed and examined in conjunction with direct numerical simulations. The purpose is to seek a possible unified explanation of the source terms that dominate the exponential evolution of the second mode. In the considered Mach 6 flow state, all three approaches consistently point to the same local energy amplification route driven by two pronounced source terms: the dilatation term in the near-wall region and the Reynolds thermal stress term or heat exchange term across the outer layer region, depending on the selection of the specific energy norm. The mathematical forms of the corresponding sources are derived or discussed explicitly. Theoretical and simulation results provide a unified understanding of the local energy amplification mechanisms of the second mode.

I. INTRODUCTION

One of the main challenges to the careful design of hypersonic vehicles is the prediction of the laminar–turbulent boundary layer transition, which results in a considerably high aerothermal load and friction drag.[1] Since the intensity of freestream turbulence in a flight environment is relatively weak, transitions tend to arise from the exponential amplification of unstable modes in hypersonic boundary layers. The Mack second mode,[2] which behaves as acoustic rays trapped between the wall and the relative sonic line,[2,3] is the dominant linear instability in hypersonic boundary layers when the Mach number exceeds a threshold value. The modal synchronization mechanism, initially proposed by Fedorov *et al.*,[4–6] and verified by Ma and Zhong[7–9] using DNS, is generally recognized as the receptive origin of the second mode. The fast and slow modes in the vicinity of the leading edge, whose phase speeds asymptotically approach those of the freestream fast and slow acoustic waves, respectively, synchronize and give rise to a new branch of the discrete spectrum. The second mode is thus excited through the intermodal interaction. In addition, the second mode can also be generated through disturbances inside the entropy layer for blunted models,[10–13] which shows a different synchronization mechanism. Although the receptivity of the second mode is well established, the growth mechanism, or how to sustain the local exponential growth from an energy-based perspective, still requires convincing explanations.

The energy source and the associated growth mechanism of the second mode have been discussed, starting from various types of stability or energy equation systems. Based on an inviscid Lagrangian formulation, Kuehl[14] examined the acoustic impedance of the second mode in the wall-normal direction. The impedance for the second mode was found to peak close to the sonic line. As a result, an acoustic impedance well that can sustain the second-mode wave resonation is formed between the sonic line and the wall. The energy required to keep the resonant standing waves in place was believed to be supplied by thermoacoustic Reynolds stress and thermodynamic effort. The importance of the thermodynamic effort was also reported in experimental investigation[15,16] on the second mode. Similar to the generation of acoustic waves depending upon the phase of the resonance process in Rijke tube,[17] the second mode behaves as trapped waves between

the relative sonic line and the wall. Therefore, the phase distribution of the source terms may play a vital role in sustaining the growth of the second mode. Tian and Wen[18] performed a relative phase analysis based on the rate of change of perturbations and the source terms to reveal the growth mechanisms of the second-mode instability. They concluded that the change of fluctuating internal energy is sustained by the advection of perturbed thermal energy in the vicinity of the critical layer and by the dilatation fluctuation near the wall. Recently, Chen *et al.*[19] extended the employment of relative phase theory to the other boundary-layer instabilities and achieved a satisfactory consistency with Kuehl's theory.

In order to fully understand the energy production and transfer of the second mode, the physical-based feature extraction method[20] is useful to provide new insights.[21,22] For a uniform base flow field, Kovásznay[23] decomposed the fluctuation into three components, i.e., vortical, acoustic, and thermal (or entropic) ones. When it comes to a non-uniform baseflow, the gradients of velocity and temperature contribute to the coupling between all three of Kovásznay's modes. This feature renders it hard to extend the application of Kovásznay's decomposition to the problem in hypersonic boundary layers with strong mean flow gradients. The momentum potential theory (MPT) proposed by Doak[24,25] overcomes the restriction in Kovásznay's approach for a general time-stationary flow. The MPT has been employed in explaining the generation process of sound waves for a cold Mach 1.3 jet flow, where the shear layer growth and breakdown process are adequately captured by its vortical component.[26] Recently, Unnikrishnan and Gaitonde[27] utilized MPT to decompose the second mode into its vortical, acoustic, and entropic components. The three components were observed to interact with the base flow in a well-described manner. The entropic component was recognized to be the most likely part of the energy source term for acoustic perturbation growth. The discovery made by Unnikrishnan and Gaitonde is instructive. Subsequently, Long *et al.*[28,29] derived a more explicit formulation of Doak's energy budget equation, which briefly contained the interaction terms among the three MPT components. The effects of various source terms on each energy flux were shown explicitly, and how various MPT components transferred energy was displayed. The positive acoustic source transferred from the vortical component was found to be the most pronounced near the critical layer. The outward transport of the acoustic component was also observed to be linked with the "sound radiation" of the supersonic mode. Although MPT has shed new insights into the boundary layer instability problem, confusion still exists due to the complicated formulation of this approach. For example, the pressure dilatation term, which was proved to be important by RPA and Lagrangian approaches, as well as experimental results, is not easily found in the governing equation of MPT. This makes MPT disconnected from other well-established methods. Improved explanations may be given by further analysis.

Remarkable progress has been made through the analysis of classical acoustic energy,[14] the relative phase analysis in the perspective of resonance,[18,19] and the feature extraction approach of momentum potential theory.[27] However, existing theories have not yet reached a consensus owing to differences in the specific form of governing equations. Despite the fact that Chen *et al.*[19] reported consistencies between the relative phase analysis and the thermoacoustic interpretation, the MPT was not included and thus disconnected from the existing framework. Therefore, a more comprehensive and self-consistent explanation of the energy source responsible for the second-mode growth is required and necessary. In the present study, the source term effects, which are related to the local destabilization of the second mode, are theoretically analyzed with direct numerical simulations. Comparative studies on the source terms from three influential theoretical approaches are conducted, and the connection of these approaches is discussed in detail. Eventually, a unified explanation of significant energy sources for the local amplification of the second mode is deduced. This paper incorporates the MPT tool into the energy-based theoretical framework. Furthermore, the detailed derivation of the Lagrangian equations to include the heat exchange effect is provided for the first time, which facilitates complete considerations from energy perspectives.

The remainder of the paper is organized as follows: Section II describes the three energy analysis methods and simulation strategies of the DNS. Section III presents the base flow and the evolution of the second-mode instability. The dominant energy source terms of the second mode are derived or identified for three energy analysis methods. Section IV describes a consistent energy-based framework of amplification mechanisms for the second mode. Section V gives concluding remarks.

II. METHODOLOGY

A. Revisit of three energy analysis methods

1. Relative phase analysis

Relative phase analysis (RPA) employed here is originally utilized to interpret how acoustic waves are generated in the Rijke tube through a resonance process.[17] Similar to that, the second mode demonstrates the reflective acoustic nature and behaves as compression and expansion waves between the relative sonic line and the wall. To identify the pronounced sources and explain the growth mechanisms of the second mode, Tian and Wen[18] employed RPA to study the local phase discrepancy between the rate of change of fluctuations and right-hand-side source terms. Since the two-dimensional second mode is more energetic than the three-dimensional one, the former is considered in our study. In linear stability analysis, which neglects the effects of non-parallel and nonlinear terms, the quantities are decomposed into the time-averaged terms $\overline{\phi}$ and disturbed quantities ϕ'. Furthermore, the disturbance term can be written as the form of traveling waves,

$$\phi = \overline{\phi} + \phi', \quad \phi' = \hat{\phi}(y)e^{\mathrm{i}(\alpha x - \omega t)} + c.c., \tag{1}$$

where ϕ is $[u, v, T, p]^{\mathrm{T}}$, $\hat{\phi}$ represents the corresponding complex eigenfunctions, u, v, T, and p denote the streamwise velocity, wall-normal velocity, temperature, and pressure, respectively, and the superscript 'T' denotes the transpose. In addition, t is the time, α is the streamwise wavenumber, ω is the angular frequency, x and y are Cartesian coordinates in streamwise and wall-normal directions, respectively, and $c.c.$ denotes complex conjugate. Note that in the spatial analysis, α is a complex number whose imaginary part corresponds to the spatial growth rate, while ω is a real number. The solution of the disturbance can be either extracted from downstream DNS data or provided by the linear stability theory (LST), where an eigenvalue problem is solved by our well-validated in-house LST code.[30–33] In this paper, the DNS data are mainly used for RPA, which serves to confirm the LST results by Tian and Wen.[18]

Generally, for the second mode under adiabatic wall condition, the magnitude of the eigenfunction of temperature fluctuation is observed to be significantly larger than that of velocity fluctuation, as reported by Erlebacher and Hussaini.[34] Therefore, in the relative phase analysis, the change of internal energy perturbation is of interest. The reduced dimensionless linearized internal energy equation obtained by Tian and Wen[18] is employed. For reading convenience, it is rewritten in the dimensional form as

$$\underbrace{\mathrm{i}(\alpha\overline{u}-\omega)\frac{\hat{T}}{\overline{T}}}_{G}=\underbrace{\mathrm{i}\alpha\overline{u}\frac{\hat{T}}{\overline{T}}}_{G_1}\underbrace{-\mathrm{i}\omega\frac{\hat{T}}{\overline{T}}}_{G_2}$$
$$=\underbrace{-\frac{d\overline{T}}{dy}\frac{\hat{v}}{\overline{T}}}_{P_1}\underbrace{-(\gamma-1)\left(\mathrm{i}\alpha\hat{u}+\frac{d\hat{v}}{dy}\right)}_{P_2}+\underbrace{\frac{\kappa(\gamma-1)}{\overline{p}}\frac{d^2\hat{T}}{dy^2}}_{P_3}+\varepsilon, \quad (2)$$

where G_1 and G_2 represent the advection and the time rate change of internal energy perturbation, respectively, and three source terms are denoted as P_1, P_2, and P_3, corresponding to wall-normal transport of internal energy (related to Reynolds thermal stress), dilatation fluctuation, and thermal conduction, respectively. In addition, κ denotes the coefficient of heat conduction, and ε represents the residual term which is negligible. In RPA, the source terms which demonstrate an approaching phase with the left-hand-side term of the governing equation positively contribute to the growth of perturbation energy.

2. Momentum potential theory

In the framework of MPT, the flow field is assumed to be time-stationary.[24,25] Under this condition, any physic quantity can be expressed as the sum of the time-averaged quantity and the fluctuating quantity. The fluctuating momentum density, $\boldsymbol{m}'=(\rho\boldsymbol{u})'$, is split into its vortical, acoustic, and thermal components, where $\boldsymbol{u}$ is a velocity vector. Consequently, the momentum density fluctuation $\boldsymbol{m}'$ can be written as the sum of the vortical component $\boldsymbol{m}'_B$, the acoustic component $\boldsymbol{m}'_A$, and the thermal component $\boldsymbol{m}'_T$

$$\boldsymbol{m}'=\boldsymbol{m}'_B+\boldsymbol{m}'_A+\boldsymbol{m}'_T. \quad (3)$$

Vortical component $\boldsymbol{m}'_B$ is solenoidal, isobaric, and isentropic. Acoustic component $\boldsymbol{m}'_A$ represents the irrotational and isentropic part of $\boldsymbol{m}'$, which is related to the pressure fluctuation p'. Thermal component $\boldsymbol{m}'_T$ represents the irrotational and isobaric part of $\boldsymbol{m}'$, which is related to the entropy fluctuation s' in the flow field. The explicit expressions of the three components can be found in Ref. 28. Consider the conservation equation of the momentum fluctuation,

$$\frac{\partial\boldsymbol{u}'}{\partial t}+\nabla H'=-\boldsymbol{\alpha}', \quad (4)$$

where H' denotes the total fluctuating enthalpy (TFE) per unit mass and $\boldsymbol{\alpha}'$ is the "acceleration" vector,

$$H'=\left(\frac{\boldsymbol{u}^2}{2}+c_pT\right)', \quad \boldsymbol{\alpha}'=\left(-\boldsymbol{\Omega}\times\boldsymbol{u}+T\nabla s+\frac{1}{\rho}\nabla\cdot\overline{\overline{\boldsymbol{S}}}\right)', \quad (5)$$

where c_p represents the specific heat at constant pressure, $\boldsymbol{\Omega}$ is the vorticity, and $\overline{\overline{\boldsymbol{S}}}$ is the viscous stress tensor. The mean transport equation of the TFE due to $\boldsymbol{m}'$ can be obtained as

$$\nabla\cdot\overline{(\boldsymbol{m}'H')}=-\overline{(\boldsymbol{m}'\boldsymbol{\alpha}')}+\frac{\overline{p'}}{R}\frac{\overline{\partial s'}}{\partial t}, \quad (6)$$

where s denotes the entropy and R represents the gas constant. The above equation can also be written as

$$\overline{\frac{\partial(\rho u)'H'}{\partial x}}+\overline{\frac{\partial(\rho v)'H'}{\partial y}}$$
$$=-(\overline{\boldsymbol{m}'_B\alpha'}+\overline{\boldsymbol{m}'_A\alpha'}+\overline{\boldsymbol{m}'_T\alpha'})+\frac{\overline{p'}}{R}\frac{\overline{\partial s'}}{\partial t}. \quad (7)$$

The left-hand side of Eq. (7) represents the transport of TFE by momentum density fluctuations. The first three terms of the right-hand side term represent the source terms due to interactions between $\boldsymbol{\alpha}'$ and different MPT components. The last term on the right-hand side represents the source term due to the thermal diffusion process. To connect the MPT with the growth rate of the second mode, Eq. (7) is integrated in the y direction. According to Ref. 29, we have $\overline{\partial(\rho u)'H'/\partial x}=-2\alpha_i\overline{(\rho u)'H'}$ and denote $\int_0^{+\infty}\overline{(\rho u)'H'}dy$ as Q_x. Since the integral of $\overline{\partial(\rho v)'H'/\partial y}$ in the y direction is zero, eventually we may obtain the growth rate of the second mode contributed by different source terms,

$$-\alpha_i=\sigma_B+\sigma_A+\sigma_T+\sigma_s. \quad (8)$$

Here,

$$\sigma_B=\frac{\int_0^{+\infty}-\overline{\boldsymbol{m}'_B\boldsymbol{\alpha}'}dy}{2Q_x}, \quad \sigma_A=\frac{\int_0^{+\infty}-\overline{\boldsymbol{m}'_A\boldsymbol{\alpha}'}dy}{2Q_x},$$
$$\sigma_T=\frac{\int_0^{+\infty}-\overline{\boldsymbol{m}'_T\boldsymbol{\alpha}'}dy}{2Q_x}, \quad \sigma_s=\frac{\int_0^{+\infty}\frac{\overline{p'}}{R}\frac{\overline{\partial s'}}{\partial t}dy}{2Q_x}. \quad (9)$$

3. Lagrangian equations

Since the second mode belongs to the family of inviscid Mack modes, the inviscid Lagrangian framework is applicable. The inviscid linearized N–S equation under the locally parallel-flow assumption can be expressed by

$$\frac{\partial\rho'}{\partial x}+v'\frac{\partial\overline{\rho}}{\partial y}+\overline{\rho}\left(\frac{\partial u'}{\partial x}+\frac{\partial v'}{\partial x}\right)=0, \quad (10)$$

$$-\frac{\partial u'}{\partial t}+\overline{u}\frac{\partial u'}{\partial x}+v'\frac{\partial\overline{u}}{\partial y}=-\frac{1}{\overline{\rho}}\frac{\partial p'}{\partial x}, \quad (11)$$

$$-\frac{\partial v'}{\partial t}+\overline{u}\frac{\partial v'}{\partial x}=-\frac{1}{\overline{\rho}}\frac{\partial p'}{\partial y}, \quad (12)$$

$$\frac{\partial s'}{\partial t}+\overline{u}\frac{\partial s'}{\partial x}+v'\frac{\partial\overline{s}}{\partial y}=0. \quad (13)$$

The relationship between the entropy fluctuation and the pressure and density fluctuations is given by

$$s'=c_v\frac{p'}{\overline{p}}-c_p\frac{\rho'}{\overline{\rho}}. \quad (14)$$

Substituting Eq. (14) into Eq. (13) yields

$$\frac{c_p}{\overline{\rho}}\frac{\partial \rho'}{\partial t}+\overline{u}c_p\frac{\partial}{\partial x}\left(\frac{\rho'}{\overline{\rho}}\right)+\frac{v'c_p}{\overline{\rho}}\frac{\partial \overline{\rho}}{\partial y} =\frac{c_v}{\overline{p}}\frac{\partial p'}{\partial t}+\overline{u}c_v\frac{\partial}{\partial x}\left(\frac{p'}{\overline{p}}\right)+\frac{v'c_v}{\overline{p}}\frac{\partial \overline{p}}{\partial y}, \tag{15}$$

where c_v represents the specific heat at constant volume. With the parallel base flow assumption, Eq. (15) can be rewritten as

$$\frac{\partial \rho'}{\partial t}+\overline{u}\frac{\partial \rho'}{\partial x}+v'\frac{\partial \overline{\rho}}{\partial y}=\frac{1}{\overline{a}^2}\left(\frac{\partial p'}{\partial t}+\overline{u}\frac{\partial p'}{\partial x}\right). \tag{16}$$

Here, $\overline{a}$ denotes the local speed of sound. Combining Eqs. (10) and (16) gives rise to

$$\frac{1}{\overline{\rho}\overline{a}^2}\left(\frac{\partial p'}{\partial t}+\overline{u}\frac{\partial p'}{\partial x}\right)+\left(\frac{\partial u'}{\partial x}+\frac{\partial v'}{\partial x}\right)=0. \tag{17}$$

Then, taking $u'\cdot$ Eq. (11) + $v'\cdot$ Eq. (12) gives

$$\left(\frac{\partial}{\partial t}+\overline{u}\frac{\partial}{\partial x}\right)\frac{\overline{\rho}(u'u'+v'v')}{2}+u'v'\overline{\rho}\frac{\partial \overline{u}}{\partial y}=u'\frac{\partial p'}{\partial x}+v'\frac{\partial p'}{\partial y}. \tag{18}$$

Finally, combining Eqs. (17) and (18) and taking time average, we obtain

$$\overline{u}\frac{\partial}{\partial x}\underbrace{\left(\overline{\overline{\rho}\frac{u'u'+v'v'}{2}+\frac{p'p'}{2\overline{\rho}\overline{a}^2}}\right)}_{\text{PAE}}=\underbrace{-\overline{\frac{\partial(p'u')}{\partial x}-\frac{\partial(p'v')}{\partial y}}}_{\text{DAP}}\underbrace{-\overline{u'v'\overline{\rho}\frac{\partial \overline{u}}{\partial y}}}_{\text{RSS}}. \tag{19}$$

The left-hand side of Eq. (19) represents the rate of change in particle acoustic energy (PAE). The first two terms on the right-hand side represent the divergence of acoustic power (DAP), and the third term on the right-hand side is the Reynolds shear stress (RSS). The above equation is equivalent to the formulation based on the acoustic energy norm by Kuehl.[14] The difference is that RSS is now considered in the present paper. Despite the fact that the second mode is of acoustic nature, the effect of the heat exchange term[23] should be important in hypersonic boundary layers. However, this term is neglected in their paper. Considering this heat exchange effect with a complete Chu's energy norm, we obtain

$$\overline{u}\frac{\partial}{\partial x}\underbrace{\left[\overline{\overline{\rho}\frac{u'u'+v'v'}{2}+\frac{p'p'}{2\overline{\rho}\overline{a}^2}+\frac{\gamma-1}{2\gamma}\overline{p}\left(\frac{s'}{R}\right)^2}\right]}_{\text{Chu's energy density}} =\underbrace{-\overline{\frac{\partial(p'u')}{\partial x}-\frac{\partial(p'v')}{\partial y}}}_{\text{DAP}}\underbrace{-\overline{u'v'\overline{\rho}\frac{\partial \overline{u}}{\partial y}}}_{\text{RSS}}\underbrace{-\overline{\frac{\overline{p}}{\overline{T}}\frac{\partial \overline{T}}{\partial y}v's'}}_{\text{HE}}. \tag{20}$$

The third term on the right-hand side represents the effect of heat exchange, noted as HE in the following analysis.

B. Direct numerical simulation

This paper investigates the hypersonic boundary layer over a flat plate with a sharp leading edge and zero attack angle. Two-dimensional patterns of the base flow and disturbance are concerned since the most unstable second mode is two-dimensional. The basic state of the hypersonic boundary layer is calculated at Mach number 6 and Reynolds number 2×10^6. The wall temperature condition is nearly adiabatic with $T_w/T_\infty=7.04$, which is the same as that by Unnikrishnan and Gaitonde.[27] In the dimensionless N–S equations, the primitive quantities are normalized by the corresponding free-stream quantities, except that the pressure is normalized by $\rho_\infty u_\infty^2$. In addition, the perfect gas model is adopted with the specific heat ratio $\gamma=1.4$ and Prandtl number $Pr=0.72$. The temperature dependence of the dynamic viscosity is modeled by $\mu/\mu_\infty=(T/T_\infty)^{0.7}$.

After the base flow is converged, a wall-blowing-suction actuator[35] is utilized to initiate the second mode. As indicated by Wang and Zhong,[36] the actuator upstream of the corresponding synchronization point ($x\sim0.14$ m) would excite the unstable evolution of the second mode. The fluctuation of the wall-normal mass flow rate q_w is given by

$$q_w(x,t)=\delta\rho_\infty u_\infty\sin\left(2\pi\frac{x-x_1}{x_2-x_1}\right)\sin(\omega t),\quad x_1\le x\le x_2, \tag{21}$$

where $x_1=0.007\,16$ and $x_2=0.0099$ m. The dimensionless angular frequency $\omega L/u_\infty$ is chosen to be 260 following Unnikrishnan and Gaitonde. The corresponding dimensional physical frequency is 163.5 kHz. The forcing amplitude $\delta=0.0006$ is adopted to guarantee the linear evolution of the disturbances.

In terms of the simulation program, our earlier study[35] has completely validated the finite difference method of DNS code. Under the same considered flow conditions, excellent convergence of mesh resolution and time step selection was demonstrated. A fifth-order upwind compact scheme is applied to discretize the inviscid flux derivatives. The sixth-order central difference method is utilized to discretize the viscous terms. A third-order Runge–Kutta scheme is employed for the time marching.

III. RESULTS AND ANALYSIS

A. Results of base flow and unsteady field

As shown in Fig. 1(a), the base flow solution obtained by the DNS code is in good agreement with that of Unnikrishnan and Gaitonde.[27] Figure 1(b) provides the wall-normal gradients of mean streamwise velocity and temperature, which respectively contribute to the formation of Reynolds shear stress and Reynolds thermal stress, and it is indicated that compared to the gradient of velocity, the temperature gradient is more prominent with a peak near the boundary layer. The wall pressure fluctuation is also compared with the reference data in Fig. 2. It is shown that the disturbance undergoes exponential growth starting from about $x=0.1$ m. The consistent result presented compared with references verified the eligibility of the computational grid adopted. Figure 3 displays the contours of p', T', and ρ' of DNS. Evident amplification is observed mainly in the near-wall region and near the critical layer. Specifically, pressure fluctuation is mainly distributed near the wall, while density and temperature fluctuations tend to be concentrated near the critical layer ($y=y_c$). Here, y_c represents the location of the critical layer where the nondimensional phase speed of the second mode equals the local base streamwise velocity. Therefore, there probably exist crucial energy sources distributed in these two regions, which are responsible for the growth of perturbation energy of the second modes.

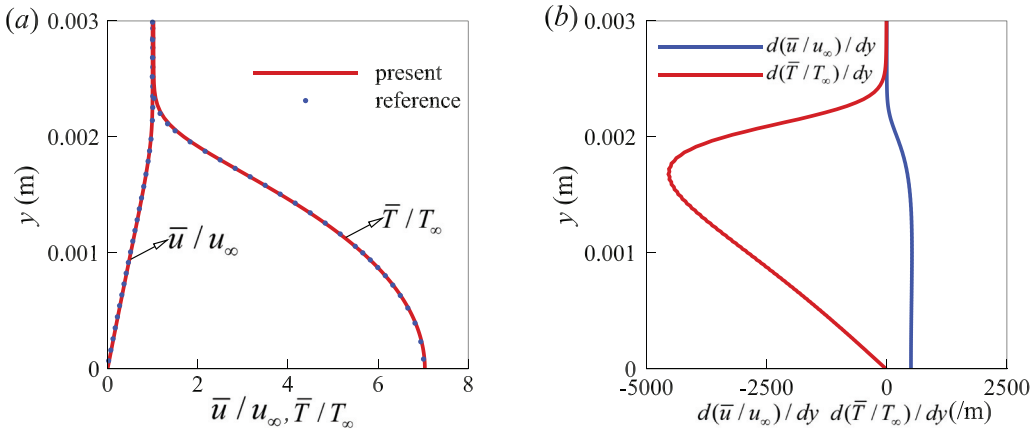

FIG. 1. Mean flow solution of (a) streamwise velocity and (b) temperature at $x = 0.18$ m compared with Ref. 27.

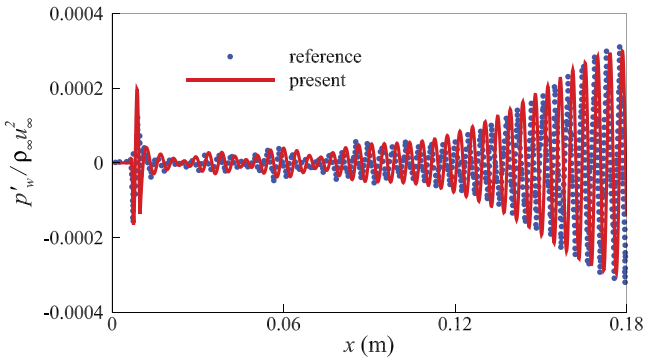

FIG. 2. Instantaneous pressure fluctuations along the wall compared with Ref. 27.

B. Results of relative phase analysis

Instantaneous DNS data are first transformed into the frequency domain via Fourier transform. For the disturbed result with a period, a temporal fast Fourier transform (FFT) analysis is performed to split the disturbances into harmonic components,

$$\phi'(x,y,t) = \hat{\phi}(x,y)e^{-i\omega t} + c.c. \tag{22}$$

Here, ten periods of the harmonic signal are used for FFT. Thus, the second-mode (fixed) frequency is 10 times the resolved lowest frequency. Meanwhile, the second-mode (single) frequency is 1/8 the Nyquist frequency, which enables the extraction of the desired second-mode component. This setup is sufficient for this simple single-frequency-disturbance case. Subsequently, the amplitude and phase profiles of the terms in Eq. (2) are obtained for the actuator frequency and are depicted in Figs. 4 and 5. Figure 4 indicates that the phase discrepancy between the time rate of change (G_1) and the advection (G_2) of the internal energy fluctuation nearly remains to be π, and their amplitudes peak near the critical layer. The antiphase relationship between G_1 and G_2 cancels each other, which results in a small-amplitude total energy growth. In terms of the relative phase, Fig. 5 demonstrates that the Reynolds-thermal-stress-related term P_1 and the dilatational term P_2 are in phase with the left-hand-side G in the near wall region (between the wall and $y = 0.3y_c$) and in the outer layer (between $y = 0.3y_c$ and $y = y_c$), respectively. Consequently, the main energy sources that sustain the second-mode growth are the dilatation effect (P_2) in the near wall region and the Reynolds thermal stress effect (P_1) in the outer layer. The distribution of amplitude and phase is consistent with that of Tian and Wen[18] obtained by LST. Therefore, the nonparallel effect is negligible in the phase analysis with regard to the second mode.

C. Results of momentum potential theory

Based on the DNS data, the MPT is employed to analyze the distribution of energy sources and the contribution to the growth rate via the decomposition in Eq. (8). The computational domain has a size of 0.2×0.05 m^2. Near the upper boundary, the magnitude of the three components of MPT is found to decay to less than 10^{-6} times the maxima in the local streamwise profile. The sponge layer is also used next to the outflow boundary to minimize the reflection of disturbances.[32] Precursor numerical simulation with extended computation domain shows no visible difference in terms of the MPT decomposition results. Figure 6 provides the amplitude distribution of the acoustic component and its flux lines, which suggests a waveguide behavior with regard to energy transport. The waveguide behavior is most clearly manifested in the acoustic component, displaying alternating monopoles along an essentially horizontal line at approximately the height of the critical layer. As a result, acoustic fluctuations are basically "locked" between the wall and the critical layer. These findings are consistent with the overall feature of the Mack mode.[37]

Based on Eq. (8) in Sec. II, the growth rate of the second mode arises from different source terms, as shown in Fig. 7. It is found that the peak position of the diffusion-related growth rate σ_s coincides with the synchronization point, in the vicinity of which the second mode is generated. Thus, the diffusion term is quite significant to the second-mode energy growth. However, the diffusion term has never been explicitly linked with the terms in either the conventional energy budget or the linear stability equation, which possess more clear physical meanings. In other words, the role of the diffusion term is not clarified

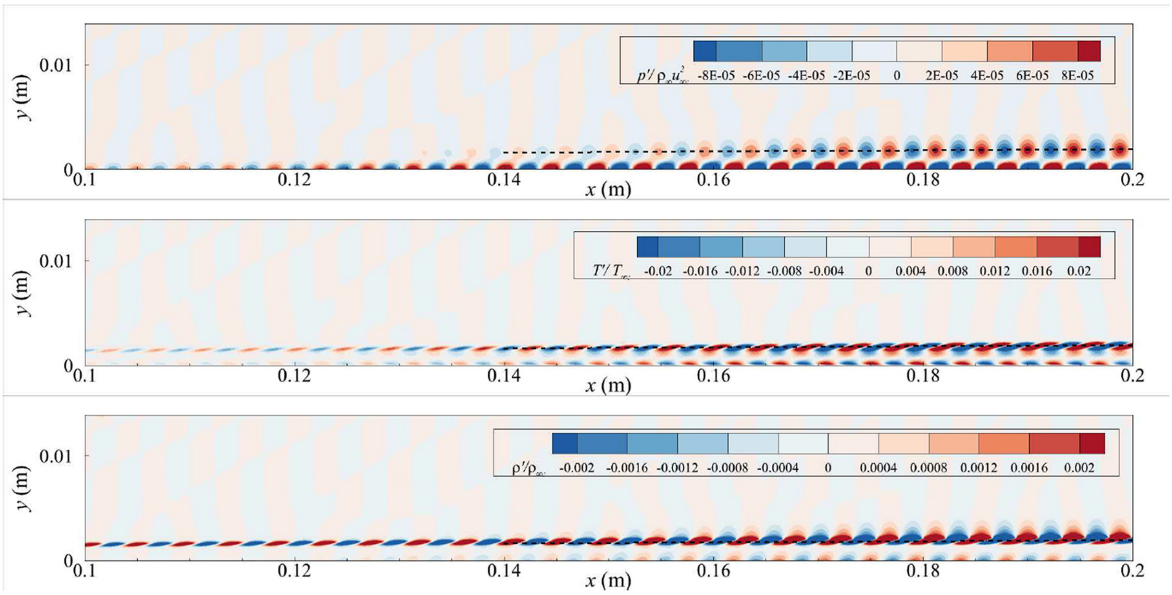

FIG. 3. Contours of pressure (top), temperature (middle), and density (bottom) fluctuations. Dashed line marks the location of the critical layer ($y = y_c$).

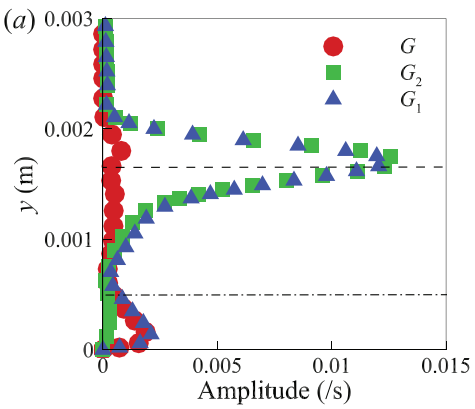

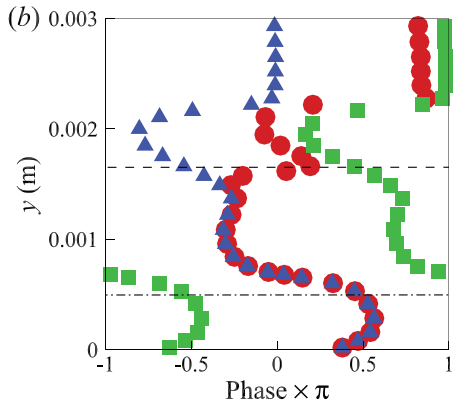

FIG. 4. (a) Amplitude and (b) phase profiles of G, G_1, and G_2 in Eq. (2) at $x = 0.16$ m. Dashed line marks $y = y_c$ and dash-dotted line marks $y = 0.3y_c$.

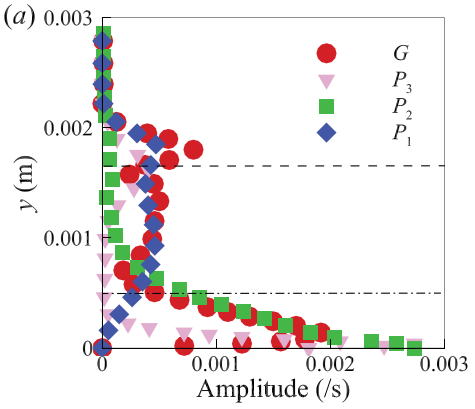

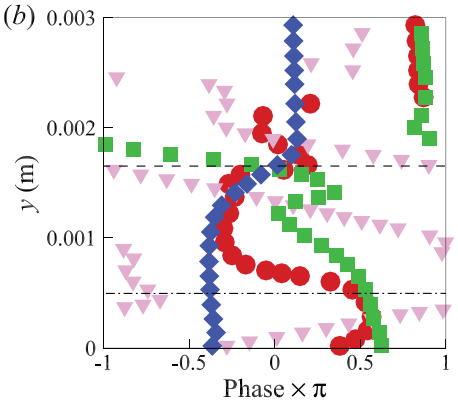

FIG. 5. (a) Amplitude and (b) phase profiles of G, P_1, P_2, and P_3 in Eq. (2) at $x = 0.16$ m. Dashed line marks $y = y_c$ and dash-dotted line marks $y = 0.3y_c$.

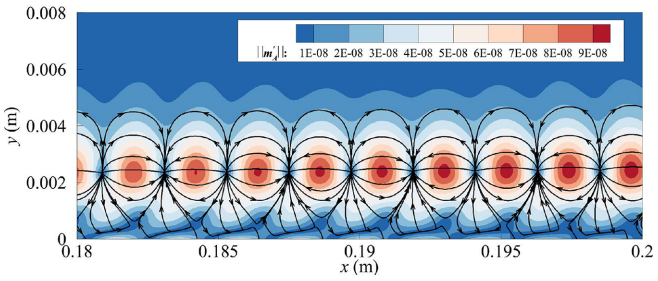

FIG. 6. Flux line and the amplitude magnitude (contour) of the acoustic component (kg/m^2/s).

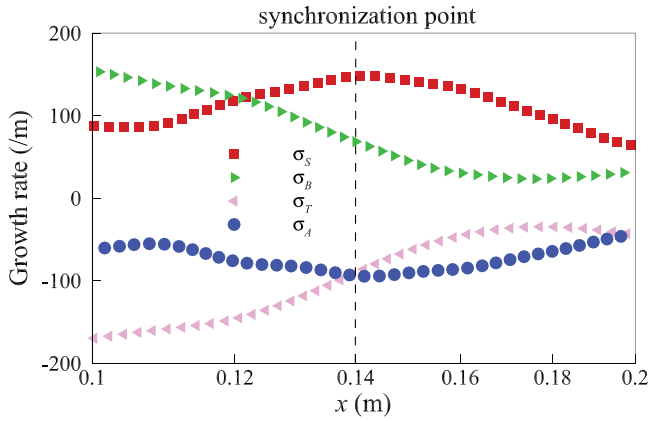

FIG. 7. Growth rate of the second mode contributed by different MPT source terms. Dashed line marked the location of the synchronization point.

from the usual viewpoint. In this paper, the relation between the diffusion term and the second mode growth mechanism is elucidated. As shown in Appendix, the expression of the thermal diffusion term can be decomposed into

$$\overline{(p'/R)(\partial s'/\partial t)} = \underbrace{\frac{\gamma}{\gamma-1}\overline{p'\nabla\cdot u'}}_{T_1} + \underbrace{\frac{\gamma}{\gamma-1}\frac{\nabla\cdot\overline{u}}{\overline{\rho}}\overline{p'\rho'}}_{T_2} + \underbrace{\frac{\gamma}{\gamma-1}\overline{\frac{p'}{\overline{\rho}}\nabla\overline{\rho}\cdot u'}}_{T_3} + \underbrace{\frac{\gamma}{\gamma-1}\overline{\frac{p'}{\overline{\rho}}\nabla\rho'\cdot\overline{u}}}_{T_4}. \quad (23)$$

In Eq. (23), the term $\frac{\gamma}{\gamma-1}\overline{p'\nabla\cdot\boldsymbol{u}'}$, noted as T_1, refers to the dilatation effect, while $\frac{\gamma}{\gamma-1}\frac{\nabla\cdot\overline{\boldsymbol{u}}}{\overline{\rho}}\overline{p'\rho'}$ is noted as T_2, represents the work done on the mean divergence by the thermodynamic fluctuations. With the parallel base flow assumption, T_3 can be rewritten as

$$\frac{\gamma}{\gamma-1}\overline{\frac{p'}{\overline{\rho}}\nabla\overline{\rho}\cdot\boldsymbol{u}'} = \frac{\gamma}{\gamma-1}\overline{\frac{p'}{\overline{\rho}}\left(\frac{d\overline{\rho}}{dy}\right)v'} = -\frac{\gamma}{\gamma-1}\overline{\frac{p'}{\overline{T}}\left(\frac{d\overline{T}}{dy}\right)v'}, \quad (24)$$

which contributes to the energy transported by the wall-normal velocity fluctuation. This term is referred to as the Reynolds thermal stress term in MPT, and the effect of Reynolds thermal stress is represented by P_1 in RPA. For the fourth term, T_4 can be split into

$$\underbrace{\frac{\gamma}{\gamma-1}\overline{\frac{p'}{\overline{\rho}}\nabla\rho'\cdot\overline{u}}}_{T_4} = \underbrace{\frac{\gamma}{\gamma-1}\frac{\overline{u}}{\overline{p}}\overline{p'\frac{\partial p'}{\partial x}}}_{T_{41}} \underbrace{-\frac{\gamma}{\gamma-1}\frac{\overline{u}}{\overline{T}}\overline{p'\frac{\partial T'}{\partial x}}}_{T_{42}}. \quad (25)$$

The profiles of the terms in Eq. (25) are depicted in Fig. 8(a), where $x=0.16$ m falls in the unstable second-mode region. It is indicated that T_4 equals T_{42} approximately. Note that the advection of perturbation of internal energy (G_1) in RPA is contained in T_{42}. Specially, G_1 corresponds to $(\overline{u}/\overline{T})\partial T'/\partial x$ in real number space, whereas the production of T_{42} results from time average of $(\overline{u}/\overline{T})\partial T'/\partial x$ and pressure fluctuation. However, the advection of perturbation of internal energy should be on the left-hand side of the energy equation and treated as a generated term. Its value is mainly distributed near the critical layer, perfectly canceled by the time rate of change of the internal energy term (G_2), as shown in Fig. 3. Therefore, to compare the result of MPT with that of RPA, this T_4 term is not treated as the source

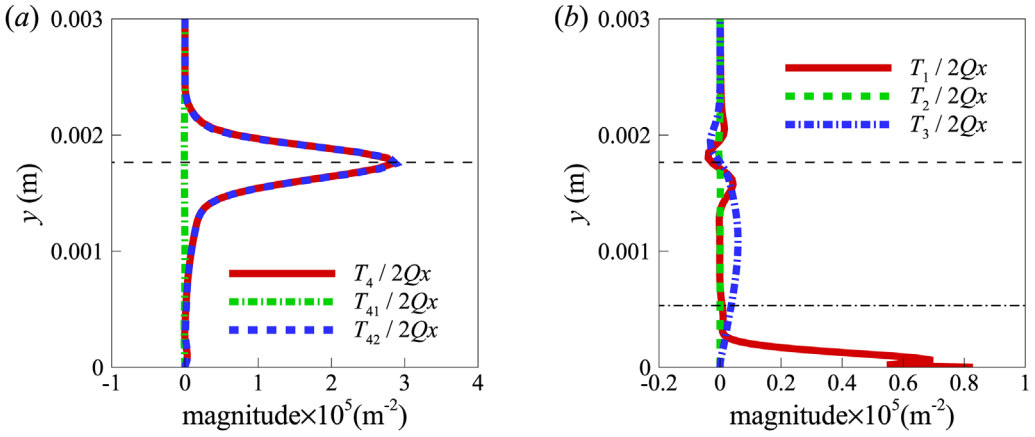

FIG. 8. Distribution of (a) T_4, T_{41}, and T_{42} and (b) T_1, T_2, and T_3 decomposed from the thermal diffusion term of MPT at $x=0.16$ m. Dashed line marks $y=y_c$ and dash-dotted line marks $y=0.3y_c$.

term. Further analysis will be performed on the other source terms, i.e., T_1, T_2, and T_3.

To explore which term plays a dominant role in contributing to the growth of the second mode, the distribution of different source terms obtained from the diffusion term of MPT is of importance, as depicted in Fig. 8(b). The pronounced dilatation effect near the wall is successfully reproduced by the subterm T_1 of the thermal diffusion in MPT, which also shares some similarities in the significance of near-wall dilatation in the wind tunnel experiment.[38] The energy transported by the wall-normal velocity fluctuation is evident in the outer region between $y = 0.3y_c$ and $y = y_c$, which resembles the distribution in Fig. 5(a). The peak near the critical layer is not evident in Fig. 8(b). To conclude, the significance of the dilatation effect is ultimately detected in the MPT framework, while that of the thermal stress effect is partly found. The remaining thermal stress effect may be originated from the terms σ_B, σ_A, and σ_T in Eq. (8), which are not easily shown in an explicit way. However, these observations do not contradict the existing knowledge because the acoustic energy amplification of the second mode due to the near-wall mechanism has been ultimately manifested in the thermal diffusion term.

D. Results of Lagrangian analysis

Based on the data of DNS, the time-averaged quantities of source terms in Eq. (20) are depicted in Fig. 9(a). It is indicated that in the near wall region, the dominant source term that destabilizes the second mode is observed to be the DAP. The RSS term keeps nearly a constant positive value inside the boundary layer, indicating a moderate destabilization effect on the second mode. However, the positive contribution of the RSS term is nearly canceled by DAP in the outer region. Near the critical layer, the heat exchange (HE) term shows a pronounced peak, indicating a substantial positive contribution to the growth of Chu's energy. The moderate distribution of RSS and distinguished role of HE may result from the diverse profile of wall-normal gradients of streamwise velocity and temperature, as shown in Fig. 1(b). The wall-normal gradient of mean temperature, which is crucial for the Reynolds thermal stress in RPA and the thermal diffusion term in MPT, is closely related to the heat exchange term in the Lagrangian equation.

To further identify the dominant source term in the near wall region, the divergence acoustic energy term is further decomposed into two terms,

$$\underbrace{\overline{\nabla \cdot (p'\boldsymbol{u}')}}_{\text{DAP}} = \underbrace{\overline{p'\nabla \cdot \boldsymbol{u}'}}_{\text{D}} + \underbrace{\overline{\nabla p' \cdot \boldsymbol{u}'}}_{\text{ND}}. \tag{26}$$

Here, $\overline{p'\nabla \cdot \boldsymbol{u}'}$ is the pressure dilatation term (D), which also represents the transport of the velocity fluctuation by the pressure fluctuation. This term vanishes in the incompressible limit with $\nabla \cdot \boldsymbol{u}' = 0$ and becomes important due to compressibility. By contrast, $\overline{\nabla p' \cdot \boldsymbol{u}'}$ is a non-dilatation term (ND), which exists in the incompressible flow. Figure 9(b) depicts the distribution of different source terms decomposed from DAP at a location after the synchronization point. The result shows that the value of the non-dilatation term equals zero on the wall and is always less than the dilatation term. Therefore, the pressure dilatation effect is dominant near the wall, while the non-dilatation one is lesser. This dilatation term eventually results in the amplification of acoustic energy of the second mode, which is consistent with the above RPA and MPT analyses.

IV. CONSISTENT ENERGY-BASED FRAMEWORK OF AMPLIFICATION MECHANISMS FOR THE SECOND MODE

A unified indicator I is defined to evaluate the contribution of the significant source terms quantitatively for the three energy source analysis methods mentioned above. In RPA, the indicator is defined as

$$I = \exp\left[-20|(\Theta_R - \Theta_L)/\Theta_L|\right], \tag{27}$$

where Θ is the phase, and the subscripts L and R denote the left-hand-side and right-hand-side terms. When the two phases are close, the indicator value approaches unity. Otherwise, the value approaches zero. The distributions of the indicator I for significant source terms in RPA, i.e., the Reynolds thermal stress (P_1) and dilatation term (P_2) are shown in Fig. 10(a). The dominance of dilatation in the near wall region and Reynolds thermal stress near the critical layer is prominent as the I indicators approach 1.0 in the corresponding region, respectively. In the MPT and Lagrangian approaches, the indicator I is defined as the ratio of each source term to the sum of source terms. As

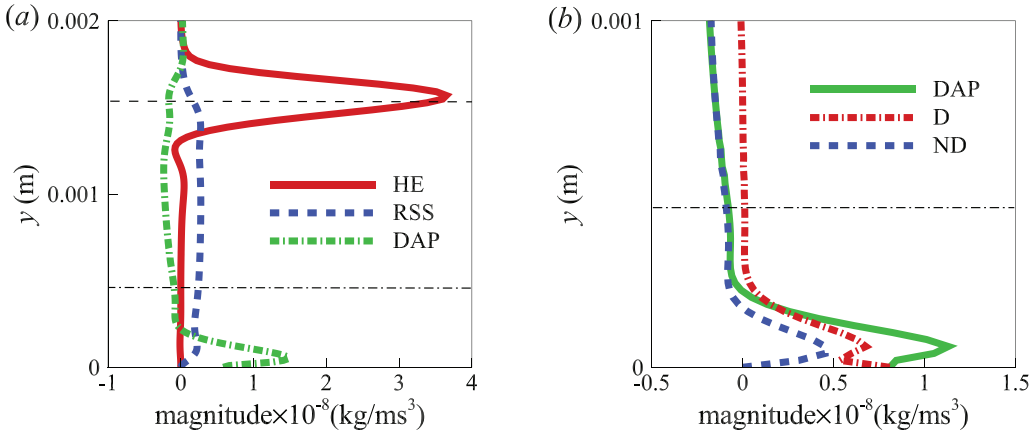

FIG. 9. Distribution of (a) DAP and RRS in Eq. (20) and (b) D and ND in Eq. (26) at $x = 0.16$ m. Dashed line marks $y = y_c$ and dash-dotted line marks $y = 0.3y_c$.

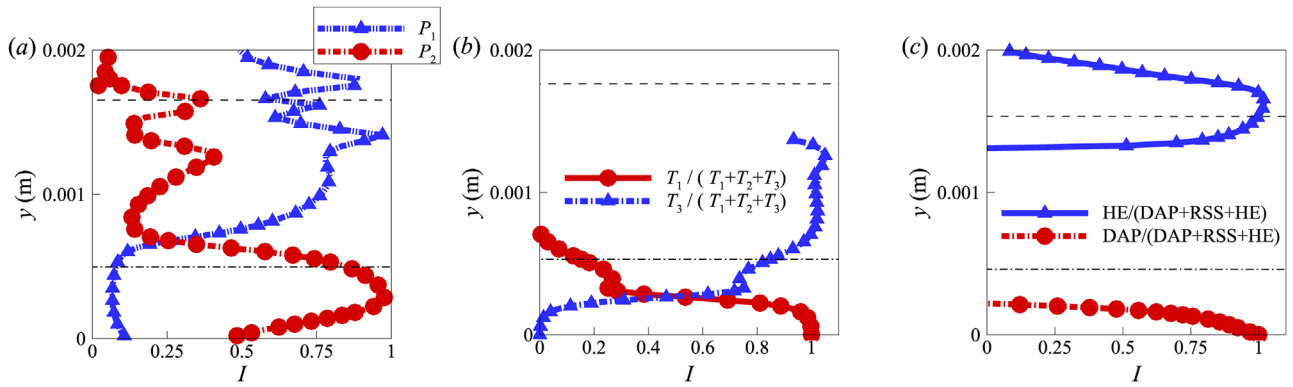

FIG. 10. *I* indicators distribution in (a) RPA, (b) MPT, and (c) Lagrangian equation at $x = 0.16$ m, respectively. Dashed line marks $y = y_c$ and dash-dotted line marks $y = 0.3y_c$.

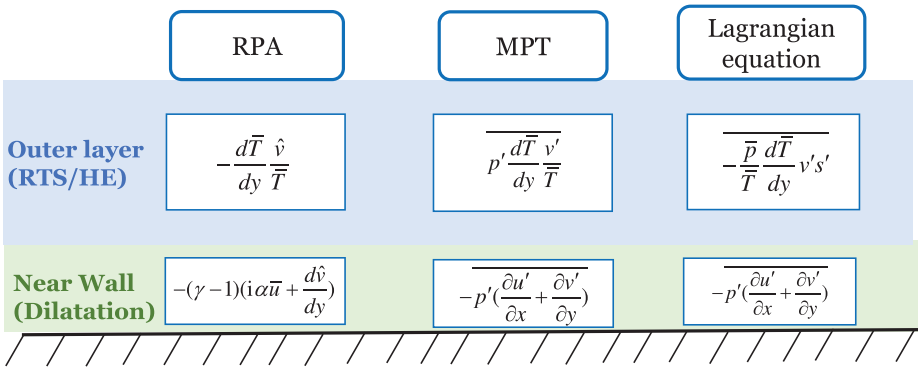

FIG. 11. A schematic of the dominant energy source terms that drive the second mode's amplification derived from three methods.

shown in Fig. 10(b), *I* indicators of the dilatation term and the RTS term in MPT approach 1.0 in the near wall region and outer layer, respectively. Also, Fig. 10(c) indicates the *I* indicators of DAP (dilatation-related term) and HE term in Lagrangian equation approach 1.0 in the near wall region and near the critical layer, respectively. Due to the sum of T_1, T_2, and T_3 approaches 0 around the critical layer, the *I* indicators are not valid in this region and, therefore, not shown.

Through the above analyses, a unified explanation of the energy source for the amplified second mode over hypersonic boundary layers is proposed. Figure 11 explicitly shows the dominant energy source terms that drive the amplification of the second mode based on the three fundamental approaches, including RPA based on the internal energy fluctuation, MPT based on the transport of TFE, and Lagrangian equation based on Chu's energy density. Basically, RPA examines the phase coherence between the rate-of-change term and the source term, while MPT and Lagrangian equation starts from the analysis of time-averaged source terms. Through a detailed decomposition and comparison of the source terms, it is found that all three approaches point to the source terms with essentially the same physical meanings. In the near-wall region below the relative sonic line, the responsible energy source is the dilatation effect, manifested as $-(\gamma-1)(\mathrm{i}\alpha\bar{u}+d\hat{v}/dy)$ in RPA and $-\overline{p'(\partial u'/\partial x+\partial v'/\partial y)}$ in MPT and Lagrangian equations. The critical role of the dilatation term in the energy transport near the wall was also reported in the flow–thermodynamics interactions analysis by Sharama and Girimaji using Helmholtz decomposition.[39] In the outer layer, both PRA and MPT report significance of the Reynolds thermal stress, which manifests as $-(d\overline{T}/dy)\hat{v}/\overline{T}$ in RPA and $\overline{(d\overline{T}/dy)p'v'/\overline{T}}$ in MPT. The dominant source term near the critical layer in the Lagrangian equation is found to be the heat exchange term, which is not considered in Kuehl's thermoacoustic interpretation. The expression of the HE term $-\overline{(d\overline{T}/dy)v's'\overline{p}/\overline{T}}$ also indicates the importance of the mean temperature gradient.

Furthermore, the Reynolds shear stress term, which appears as $-\overline{u'v'\overline{\rho}(\partial\overline{u}/\partial y)}$ in Lagrangian equations, appears to be nearly constant and moderate in the outer layer. According to the relative phase analysis of Tian and Wen[18] based on linear stability theory, the RSS term is essential in the streamwise transport of kinetic energy fluctuation of the second mode. Regarding MPT, the RSS term is probably implicitly included in the source term due to the interaction between momentum density fluctuation ($\boldsymbol{m}'$) and fluctuation acceleration term ($\boldsymbol{\alpha}'$) instead of the analyzed thermal diffusion term, since the diffusion term does not contain the mean shear $\partial\overline{u}/\partial y$.

V. CONCLUSIONS

By performing theoretical analysis and numerical simulation, the growth mechanism of the second mode across a hypersonic flat-plate boundary layer is examined. The energy source terms that drive the amplification of the second mode are investigated using three influential fundamental approaches,

including the relative phase analysis based on internal energy analysis, the momentum potential theory based on the transport of total fluctuating enthalpy, and the Lagrangian equations based on Chu's energy density. Comparative studies on the source terms from three influential theoretical approaches are conducted, and the connection of these approaches is discussed and clarified in detail. The detailed derivation of the Lagrangian equations to include the heat exchange effect is provided for the first time, which facilitates more complete considerations from energy perspectives. Meanwhile, a unified indicator is defined to evaluate the contribution of the significant source terms quantitatively.

The main finding of this paper is that the three popular fundamental approaches reach an agreement on the energy amplification mechanism of the Mack second mode. The explicit expression of each energy source is derived, and despite the mathematical form differences, the physical meanings behind them are consistent. Generally, the dilatation effect due to compressibility is responsible for the acoustic energy production near the wall, while the base temperature gradient is of significance in the wall-normal transport of internal energy in an outer region of the boundary layer. Moreover, this study focused on the second-mode instability under the adiabatic wall condition. Whether momentum potential theory can be extended to other forms of instabilities in the identification of significant source terms merits further investigation.

ACKNOWLEDGMENTS

This research was supported by the Research Grants Council, Hong Kong, under Contract Nos. 15216621 and 15204322.

AUTHOR DECLARATIONS

Conflict of Interest

The authors have no conflicts to disclose.

Author Contributions

Yifeng Chen: Formal analysis (equal); Investigation (equal); Visualization (equal); Writing – original draft (equal); Writing – review & editing (equal). **Peixu Guo:** Conceptualization (equal); Formal analysis (equal); Methodology (equal); Software (equal); Supervision (equal); Writing – original draft (equal); Writing – review & editing (equal). **Chih-Yung Wen:** Conceptualization (equal); Formal analysis (supporting); Funding acquisition (lead); Resources (lead); Supervision (equal); Writing – original draft (supporting); Writing – review & editing (supporting).

DATA AVAILABILITY

The data that support the findings of this study are available from the corresponding author upon reasonable request.

APPENDIX: DERIVATION OF EQ. (23)

The decomposition of the instantaneous quantity gives

$$\rho = \overline{\rho} + \rho', \quad \boldsymbol{u} = \overline{\boldsymbol{u}} + \boldsymbol{u}'. \tag{A1}$$

By substituting the above equation into the continuity equation, subtracting the base flow equation and dropping the nonlinear terms, it yields

$$\frac{\partial \rho'}{\partial t} + \overline{\rho}\nabla \cdot \boldsymbol{u}' + \nabla\overline{\rho} \cdot \boldsymbol{u}' + \rho'\nabla \cdot \overline{\boldsymbol{u}} + \nabla\rho' \cdot \overline{\boldsymbol{u}} = 0. \tag{A2}$$

Therefore,

$$\overline{\frac{p'}{R}\frac{\partial s'}{\partial t}} = \overline{\frac{p'}{R}\frac{\partial}{\partial t}\left(c_v\frac{p'}{\overline{p}} - c_p\frac{\rho'}{\overline{\rho}}\right)} = -\frac{\gamma}{\gamma - 1}\overline{\frac{p'}{\overline{\rho}}\frac{\partial \rho'}{\partial t}}. \tag{A3}$$

Substituting Eq. (A2) into Eq. (A3) yields

$$\overline{\frac{p'}{R}\frac{\partial s'}{\partial t}} = \frac{\gamma}{\gamma - 1}\overline{\frac{p'}{\overline{\rho}}(\overline{\rho}\nabla \cdot \boldsymbol{u}' + \nabla\overline{\rho} \cdot \boldsymbol{u}' + \rho'\nabla \cdot \overline{\boldsymbol{u}} + \nabla\rho' \cdot \overline{\boldsymbol{u}})}, \tag{A4}$$

i.e., Eq. (23).

REFERENCES

[1]J. D. Schmisseur, "Hypersonics into the 21st century: A perspective on AFOSR-sponsored research in aerothermodynamics," Prog. Aerosp. Sci. **72**, 3–16 (2015).
[2]L. Mack, "On the inviscid acoustic-mode instability of supersonic shear flows: Part 1: Two-dimensional waves," Theor. Comput. Fluid Dyn. **2**, 97–123 (1990).
[3]E. Reshotko, "Hypersonic stability and transition," in *Hypersonic Flows for Reentry Problems* (Springer-Verlag, 1991), Vol. 1.
[4]A. V. Fedorov and A. P. Khokhlov, "Excitation of unstable modes in a supersonic boundary layer by acoustic," Fluid Dyn. **26**, 531–537 (1991).
[5]A. Fedorov and A. Tumin, "Initial-value problem for hypersonic boundary-layer flows," AIAA J. **41**, 379–389 (2003).
[6]A. V. Fedorov, "Receptivity of a high-speed boundary layer to acoustic disturbances," J. Fluid Mech. **491**, 101–129 (2003).
[7]Y. Ma and X. Zhong, "Receptivity of a supersonic boundary layer over a flat plate. Part 1. Wave structures and interactions," J. Fluid Mech. **488**, 31–78 (2003).
[8]Y. Ma and X. Zhong, "Receptivity of a supersonic boundary layer over a flat plate. Part 2. Receptivity to free-stream sound," J. Fluid Mech. **488**, 79–121 (2003).
[9]Y. Ma and X. Zhong, "Receptivity of a supersonic boundary layer over a flat plate. Part 3. Effects of different types of free-stream disturbances," J. Fluid Mech. **532**, 63–109 (2005).
[10]B. Wan, C. Su, and J. Chen, "Receptivity of a hypersonic blunt cone: Role of disturbances in entropy layer," AIAA J. **58**, 4047–4054 (2020).
[11]Y. Chen, G. Tu, B. Wan, C. Su, X. Yuan, and J. Chen, "Receptivity of a hypersonic flow over a blunt wedge to a slow acoustic wave," Phys. Fluids **33**, 084114 (2021).
[12]W. Ba, M. Niu, and C. Su, "Hypersonic boundary-layer receptivity over circular cones with ellipsoidal/spherical noses," AIAA J. **61**, 518–533 (2023).
[13]M. Niu and C. Su, "Receptivity and its influence on transition prediction of a hypersonic boundary layer over a small bluntness cone," Phys. Fluids **35**, 034109 (2023).
[14]J. Kuehl, "Thermoacoustic interpretation of second-mode instability," AIAA J. **56**, 3585–3592 (2018).
[15]W. Zhu, M. Shi, Y. Zhu, and C. Lee, "Experimental study of hypersonic boundary layer transition on a permeable wall of a flared cone," Phys. Fluids **32**, 011701 (2020).
[16]W. Zhu, X. Chen, Y. Zhu, and C. Lee, "Nonlinear interactions in the hypersonic boundary layer on the permeable wall," Phys. Fluids **32**, 104110 (2020).
[17]Rayleigh, *The Theory of Sound* (Dover, New York, 1945).
[18]X. Tian and C. Wen, "Growth mechanisms of second-mode instability in hypersonic boundary layers," J. Fluid Mech. **908**, R4 (2021).
[19]Y. Chen, P. Guo, and C. Wen, "A unified explanation of energy growth sources for unstable modes in flat-plate boundary layers," J. Fluid Mech. **972**, A5 (2023).
[20]S. Unnikrishnan, "Recent advances in feature extraction techniques for high-speed flowfields," Prog. Aerosp. Sci. **140**, 100918 (2023).

[21]W. Zhu, D. Gu, W. Si, M. Zhang, S. Chen, C. Smith, Y. Zhu, and C. Lee, "Instability evolution in the hypersonic boundary layer over a wavy wall," J. Fluid Mech. **943**, A16 (2022).
[22]W. Zhu, D. Gu, W. Si, S. Chen, Y. Zhu, and C. Lee, "Reduced aerodynamic heating in a hypersonic boundary layer by a wavy wall," Sci. Bull. **67**, 988 (2022).
[23]L. S. Kovasznay, "Turbulence in supersonic flow," J. Aeronaut. Sci. **20**, 657–674 (1953).
[24]P. Doak, "Momentum potential theory of energy flux carried by momentum fluctuations," J. Sound Vib. **131**, 67–90 (1989).
[25]P. E. Doak, "Fluctuating total enthalpy as the basic generalized acoustic field," Theor. Comput. Fluid Dyn. **10**, 115–133 (1998).
[26]S. Unnikrishnan and D. V. Gaitonde, "Acoustic, hydrodynamic and thermal modes in a supersonic cold jet," J. Fluid Mech. **800**, 387–432 (2016).
[27]S. Unnikrishnan and D. V. Gaitonde, "Interactions between vortical, acoustic and thermal components during hypersonic transition," J. Fluid Mech. **868**, 611–647 (2019).
[28]T. Long, Y. Dong, R. Zhao, and C. Wen, "Mechanism of stabilization of porous coatings on unstable supersonic mode in hypersonic boundary layers," Phys. Fluids **33**, 054105 (2021).
[29]T. Long, P. Guo, R. Zhao, C. Wen, and F. Ji, "Energy growth of vortical, acoustic, and entropic components of the second-mode instability in the hypersonic boundary layer," Phys. Fluids **35**, 054104 (2023).
[30]P. Guo, Z. Gao, C. Jiang, and C. Lee, "Linear stability analysis on the most unstable frequencies of supersonic flat-plate boundary layers," Comput. Fluids **197**, 104394 (2020).
[31]P. Guo, Z. Gao, C. Jiang, and C. Lee, "Sensitivity analysis on supersonic-boundary-layer stability subject to perturbation of flow parameters," Phys. Fluids **33**, 084111 (2021).
[32]P. Guo, F. Shi, Z. Gao, C. Jiang, C. Lee, and C. Wen, "Heat transfer and behavior of the reynolds stress in Mach 6 boundary layer transition induced by first-mode oblique waves," Phys. Fluids **34**, 104116 (2022).
[33]P. Guo, F. Shi, Z. Gao, C. Jiang, C. Lee, and C. Wen, "Sensitivity analysis on supersonic-boundary-layer stability: Parametric influence, optimization, and inverse design," Phys. Fluids **34**, 104113 (2022).
[34]G. Erlebacher and M. Hussaini, "Numerical experiments in supersonic boundary-layer stability," Phys. Fluids A **2**, 94–104 (1990).
[35]R. Zhao, C. Wen, X. Tian, T. Long, and W. Yuan, "Numerical simulation of local wall heating and cooling effect on the stability of a hypersonic boundary layer," Int. J. Heat Mass Transfer **121**, 986–998 (2018).
[36]X. Wang and X. Zhong, "Effect of wall perturbations on the receptivity of a hypersonic boundary layer," Phys. Fluids **21**, 044101 (2009).
[37]A. Fedorov, "Transition and stability of high-speed boundary layers," Annu. Rev. Fluid Mech. **43**, 79–95 (2011).
[38]Y. Zhu, X. Chen, J. Wu, S. Chen, C. Lee, and M. Gad-el Hak, "Aerodynamic heating in transitional hypersonic boundary layers: Role of second-mode instability," Phys. Fluids **30**, 011701 (2018).
[39]B. Sharma and S. S. Girimaji, "Effect of flow-thermodynamics interactions on the stability of compressible boundary layers: Insights from Helmholtz decomposition," J. Fluid Mech. **962**, A18 (2023).